Bulk materials made of silicon cage clusters doped with Ti, Zr, or Hf

2010 J. Phys.: Condens. Matter 22 035501

(http://iopscience.iop.org/0953-8984/22/3/035501)

J. Phys.: Condens. Matter **22** (2010) 035501 (7pp) doi:10.1088/0953-8984/22/3/035501

Bulk materials made of silicon cage clusters doped with Ti, Zr, or Hf

C L Reis and J M Pacheco

ATP Group, CFTC and Departamento de Física da Faculdade de Ciências, Complexo Interdisciplinar da Universidade de Lisboa, Avenida Professor Gama Pinto 2, P-1649-003 Lisboa, Portugal

E-mail: clr@cii.fc.ul.pt

Received 6 August 2009, in final form 18 October 2009
Published 21 December 2009
Online at stacks.iop.org/JPhysCM/22/035501

Abstract

We investigate the feasibility of assembling the exceptionally stable isovalent $X@Si_{16}$ (X = Ti, Zr and Hf) nanoparticles to form new bulk materials. We use first-principles density functional theory. Our results predict the formation of stable, wide band-gap materials crystallizing in HCP structures in which the cages bind weakly, similar to fullerite. This study suggests new pathways through which endohedral cage clusters may constitute a viable means toward the production of synthetic materials with pre-defined physical and chemical properties.

(Some figures in this article are in colour only in the electronic version)

1. Introduction

The synthesis of new materials using suitable nano-structures constitutes a main challenge in nanotechnology. The properties of such nano-structures which enable a successful synthesis of stable bulk materials are not yet completely understood, despite the recent advances [1, 2].

In this quest, considerable attention has been paid to silicon and silicon clusters, given the technological importance of this element in the development of electronic devices [3]. Physical limits to the miniaturization of devices based on bulk silicon have already been met in the recent 45 nm generation of devices, where a high-k dielectric material such as HfO_2 has replaced SiO_2 as a gate insulator [4] for the first time in the history of integrated circuits. Contrary to fullerene-like carbon clusters, pure silicon clusters have been found to be chemically reactive, precluding the synthesis of cluster assembled materials [1]. On the other hand, early experiments by Beck [5, 6] indicated the feasibility of using metal atoms to nucleate silicon atoms into stable $X@Si_n$ clusters, of which $X@Si_{16}$ was found to be particularly stable. Recent experimental [1, 7–14] and theoretical [15–23] work has confirmed these results for a variety of mixed metal–silicon sandwich [7, 24] and cage [15, 16, 22, 23] clusters, and a special class of clusters with stoichiometry $X@Si_{16}$, with X a metal atom, has been identified [15] as especially stable by means of *ab initio* computer simulations. In particular, the stability of $X@Si_{16}$ (X = Ti, Zr, Hf) nanoparticles has been confirmed experimentally [12], via selective formation of neutral gas phase clusters, using a dual laser vaporization technique of pure metal and pure silicon targets in an inert helium atmosphere. An additional experimental confirmation of the synthesis of these nanoparticles has been reported recently using a magnetron co-sputtering technique [14]. An important feature of this class of clusters is the fact that most of the valence electronic charge density is pulled into the interior of the cage, conferring them an appreciable amount of chemical inertia. The $Ti@Si_{16}$ nanoparticle, in particular, has been the subject of considerable attention.

In a previous work [25] we investigated the possibility of using this remarkably stable cluster to synthesize a stable molecular solid. In this work we extend our previous results to include the especially stable clusters $Zr@Si_{16}$ and $Hf@Si_{16}$. The fact that Zr and Hf are isovalent to Ti provides an intuitive basis for expecting that bulk materials using $Zr@Si_{16}$ and $Hf@Si_{16}$ as constituent units are also feasible. However, we have found [25] that the feasibility of bulk $Ti@Si_{16}$ relied on a detailed interplay between intra- and inter-cage binding. Consequently, a careful analysis is needed before any conclusions can be drawn. Furthermore, by changing the nature of the nucleating element, one introduces an additional handle with which to fine-tune the structural and electronic properties of these materials. The extent to which one can profit from these extra degrees of freedom will be addressed here as well.

Using first-principles computer simulations within density functional theory we investigate the main electronic properties of $Zr@Si_{16}$ and $Hf@Si_{16}$ clusters and cluster assembled bulk forms. We show the feasibility of using the clusters as elementary building blocks to synthesize stable bulk materials, and find that all the $X@Si_{16}$ (X = Ti, Zr and Hf) cluster assembled materials crystallize in hexagonal closed packed structures (HCP). We further characterize the main structural and electronic properties of these materials, while illustrating their differences. We predict that these materials should be possible to stabilize in a metastable phase at room temperature and normal pressure conditions. This phase is predicted to be maintained under isotropic compression up to ∼1 GPa. Similar to $Ti@Si_{16}$, both $Zr@Si_{16}$ and $Hf@Si_{16}$ are especially stable semiconductors with GGA (see below) band gaps of 1.6 eV, 0.3 eV larger than that previously found for bulk $Ti@Si_{16}$.

This paper is organized as follows: in section 2 details of the method and simulations carried out are provided. Results and discussion are left to section 3, whereas the main conclusions and future prospects are postponed to section 4.

2. Methods

All *ab initio* calculations were performed within the generalized gradient approximation (GGA [26]) to density functional theory (DFT) using norm-conserving pseudopotentials [27] and a plane-wave basis [28, 29]. An energy cutoff of 30.0 hartree (816 eV) was used throughout, leading to well converged forces within 0.02 eV $bohr^{-1}$. This value was also used as a stopping criteria for structural optimizations. Large energy cutoffs are crucial to ensure reliable results (and good convergence of the forces). We note that if less restrictive (and consequently, less computer demanding) parameters are used in structural optimizations the forces (gradients of the energy with respect to atomic positions) will be poorly determined. As a consequence artificial structures and cage breakup can be obtained using $X@Si_{16}$ clusters as building blocks.

2.1. Isolated Clusters

2.1.1. Structural optimization. The atomic coordinates of the isolated clusters were computed employing a supercell hexagonal lattice with parameters $a = c = 27.0$ bohr to avoid mirror-image interactions. To ensure proper structure determination we performed several Langevin quantum molecular dynamics [30] (LQMD) simulations at different temperatures starting from arbitrary configurations of Si atoms always nucleated around the central metal atom. Subsequently we performed geometry optimizations employing a conjugated gradient algorithm starting from the lowest energy configurations obtained in the LQMD runs.

2.1.2. Electronic properties. We computed the total energy, the one-electron Kohn–Sham levels as well as the total valence electronic density $\rho(\boldsymbol{r})$ of each nano-structure at the equilibrium configuration. From the electronic density $\rho(\boldsymbol{r})$ we constructed the radial electronic density, $\rho(r) = \rho(|\boldsymbol{r}|)$ by calculating its average over the solid angle:

$$\rho(r) = \frac{1}{4\pi}\int_{\Omega}\rho(\boldsymbol{r})\,\mathrm{d}\Omega.$$

The number of valence electrons is given by

$$N = \int \mathrm{d}^3r\,\rho(\boldsymbol{r}) = \int_0^{\infty}\mathrm{d}r\,4\pi r^2\rho(r) \equiv \int_0^{\infty}\mathrm{d}r\,\eta(r). \quad (1)$$

The quantity $\eta(r)$ defined in the last integral can be useful in quantifying the electronic density inside the nanoparticle, providing a qualitative measure of its chemical inertia.

We computed the cohesive energy *per atom* for each cluster subtracting from the total energy E_{tot} the atomic energies $E_{\mathrm{ps}}^{\mathrm{Si}}$ and $E_{\mathrm{ps}}^{\mathrm{X}}$ (X = Ti, Zr, Hf) of the pseudopotential calculation, $E_{\mathrm{coh}} = (E_{\mathrm{tot}} - 16E_{\mathrm{ps}}^{\mathrm{Si}} - E_{\mathrm{ps}}^{\mathrm{X}})/17$.

2.2. Bulk phase

2.2.1. Structural optimization. In a first step, we investigate bulk forms of cluster assembled materials, using the equilibrium structures of the isolated cages. To this end, we computed the cohesive energy per cluster varying the distance between clusters in a given bulk structure, while freezing the cluster geometry and the angles between primitive lattice vectors. The cohesive energy per cage in the bulk $E_{\mathrm{coh}}^{\mathrm{b}}$ is defined as

$$E_{\mathrm{coh}}^{\mathrm{b}} = (E_{\mathrm{tot}}^{\mathrm{b}} - N_{\mathrm{c}}E_{\mathrm{I}})/N_{\mathrm{c}},$$

where $E_{\mathrm{tot}}^{\mathrm{b}}$ is the total energy per unit cell, E_{I} is the energy of the isolated cluster and N_{c} is the number of clusters in the unit cell. Several bulk structures were investigated: simple cubic (SC), diamond-type (DIA), body centred cubic (BCC), face centred cubic (FCC) and hexagonal close packed (HCP). We placed 1 cluster per unit cell in the SC, BCC and FCC structures, and 2 in DIA and HCP. We have also tried to use supercells for different lattices, but the corrections in energy were found to be negligible. We have carefully chosen the k-point sampling in each calculation (particularly for small inter-cluster distances) in order to ensure well converged results. We used the following Monkhorst–Pack grids: $2 \times 2 \times 2$ for DIA, $4 \times 4 \times 4$ for SC, BCC and FCC and $3 \times 3 \times 2$ for HCP.

Subsequently we performed a full geometry relaxation of both atomic coordinates and lattice parameters taking as a starting point the configuration corresponding to the minimum of the cohesive energy per cluster as a function of distance between clusters for the different bulk structures we found before.

2.2.2. Pressure curve and bulk modulus. Given the cohesive energy per cluster as a function of the distance d between clusters, $E_{\mathrm{coh}}(d)$, we can obtain the pressure as a function of inter-cage distance $P(d)$ by computing the numerical derivative from a cubic spline fit to the cohesive energy points:

$$P(d) = -\frac{\partial E}{\partial V} = -\frac{\partial E}{\partial d}\left(\frac{\partial V}{\partial d}\right)^{-1}.$$

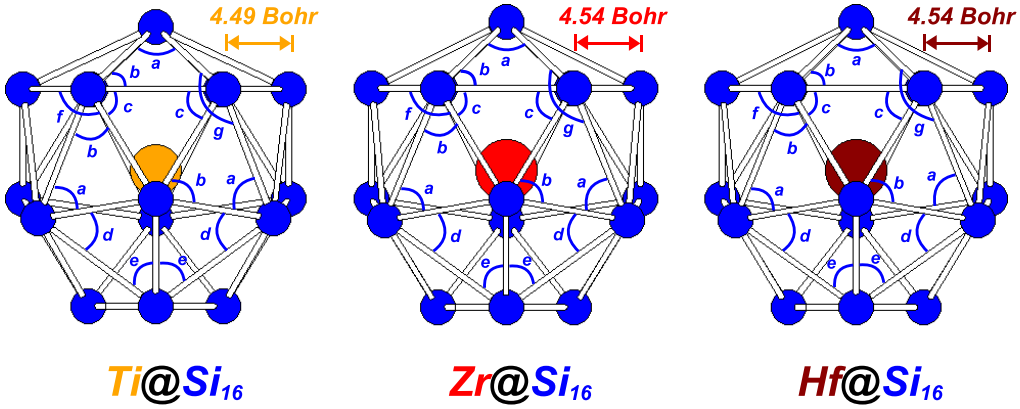

Figure 1. The Frank–Kasper [32] cage structures, corresponding to the equilibrium of the X@Si_{16} nanoparticles. These highly symmetric structures, exhibiting several C_3 symmetry axes, will be used as building blocks of molecular solids. Selected bond angles are also represented. Angle values are given in table 1.

Table 1. Selected bond angles depicted in figure 1 for the X@Si_{16} clusters (X = Ti, Zr, Hf). Similar values for the angles have been identified in amorphous silicon [33].

X@Si_{16}	*a* (deg)	*b* (deg)	*c* (deg)	*d* (deg)	*e* (deg)	*f* (deg)	*g* (deg)
Ti	54.6	62.7	60.0	53.1	63.4	120.0	106.4
Zr	54.0	63.0	60.0	52.6	63.7	120.0	108.4
Hf	54.0	63.0	60.0	52.6	63.7	120.0	108.4

For a hexagonal lattice in the ideal packing structure (HCP), the volume of the primitive cell is $V = \sqrt{2}d^3$. Thus,

$$P(d) = -\frac{1}{3\sqrt{2}d^2}\frac{\partial E}{\partial d} = -\frac{254.845}{d^2}\frac{\partial E}{\partial d}, \qquad (2)$$

which provides the pressure in GPa for lengths in bohr and energies in eV. The Bulk modulus B is determined by fitting the cohesive energy points to the Birch–Murnaghan equation of state [31]:

$$E(V) = E_0 + \frac{9V_0B_0}{16}\left\{\left[\left(\frac{V_0}{V}\right)^{\frac{2}{3}} - 1\right]^3 B_0' + \left[\left(\frac{V_0}{V}\right)^{\frac{2}{3}} - 1\right]^2\left[6 - 4\left(\frac{V_0}{V}\right)^{\frac{2}{3}}\right]\right\}. \qquad (3)$$

3. Results and discussion

3.1. Isolated clusters

The structures of the isolated X@Si_{16} nanoparticles obtained using the procedure outlined in the previous section are shown in figure 1.

All these nanoparticles exhibit Frank–Kasper [32] cage structures with C_{3v} symmetry. In table 2 the parameters characterizing the structural properties of these clusters are given. We choose three sets of distances: the distance from the metal atom to the four silicon atoms on the tetrahedral sites r_1; the distance from the metal atom to the remaining twelve silicon atoms r_2, and the minimum nearest neighbour Si–Si distance $r_{\min}^{nn}$. The Zr@Si_{16} and Hf@Si_{16} have larger dimensions than Ti@Si_{16}: r_1 and r_2 are 3% and 1% larger than the ones found for Ti@Si_{16}.

Table 2. Structural parameters for the X@Si_{16} clusters with X = Ti, Zr, Hf. r_1 is the distance from the metal atom to the four silicon atoms on the tetrahedral sites, r_2 is the distance of the metal atom to the remaining twelve silicon atoms and $r_{\min}^{nn}$ is the minimum nearest neighbour Si–Si distance.

X@Si_{16}	r_1 (bohr)	r_2 (bohr)	$r_{\min}^{nn}$
Ti	4.93	5.34	4.49
Zr	5.09	5.40	4.54
Hf	5.09	5.40	4.54

Table 3. Cohesive energy per cluster and HOMO–LUMO gaps for the X@Si_{16} clusters with X = Ti, Zr, Hf.

X@Si_{16}	E_{coh}/atom (eV)	H–L gap (eV)
Ti	−4.96	2.3
Zr	−4.99	2.4
Hf	−4.97	2.5

Once the ground state geometries have been determined, we computed their main electronic properties. In table 3 we list the calculated cohesive energy per atom and HOMO–LUMO (highest occupied–lowest unoccupied molecular orbital) gap for these clusters. Whereas the cohesive energies are almost identical for all cages the Zr@Si_{16} Hf@Si_{16} gaps are ∼6% larger than the one found for Ti@Si_{16}.

In figure 2 we show the radial electronic density of all the three clusters, which is remarkably similar. Besides their large HOMO–LUMO gaps, another indication of stability in these clusters is that almost all of the electronic density is concentrated inside the cage clusters. The vertical bars represent the outer limits of the cage cluster, taking into account the cage radius and the silicon atomic radius (cf table 2). ∼96% of the electronic charge density is concentrated inside a sphere of radius 8 bohr, suggesting a remarkable level of chemical inertia.

In figure 3 we display the one-electron energy levels. The three nanoparticles exhibit energy level distributions which are qualitatively similar. The degeneracies of the energy levels can

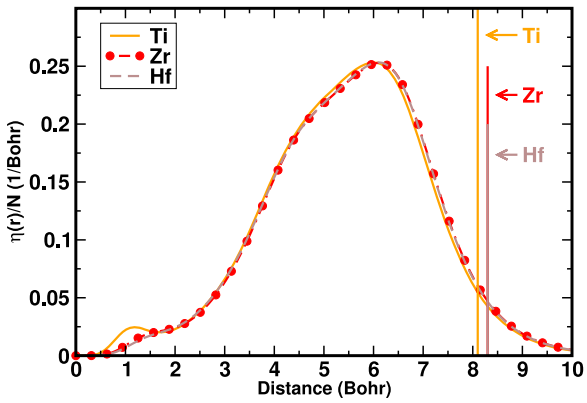

Figure 2. Normalized radial electronic densities $\eta(r) = 4\pi r^2 \rho(r)$ plotted as a function of the distance to the central metal atom for isolated clusters Ti@Si_{16} (orange, solid line), Zr@Si_{16} (red, dash–dotted line) and Hf@Si_{16} (brown, dashed line). The radial electronic density $\rho(r)$ is obtained from the calculated ground state total electronic density $\rho(r)$ taking its average over the solid angle Ω. See equation (1). The total area subtended by each curve is 1.

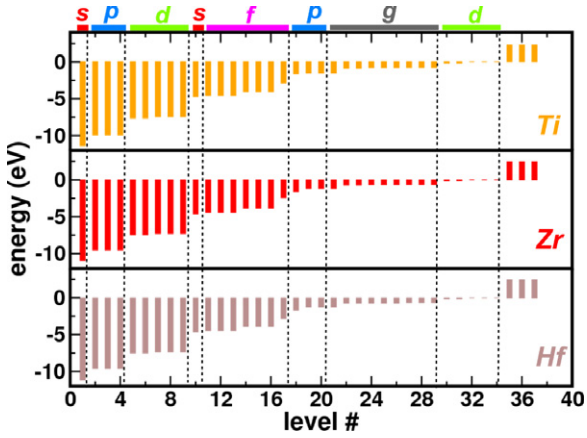

Figure 3. Energy levels for the X@Si_{16} clusters with X = Ti, Zr, Hf. The electronic occupancy of each level is 2. The plotted levels are grouped according to their approximated degeneracies corresponding to levels in a spherical (jellium) shell structure with angular momenta s, p, d, s, f, p, g, d.

be qualitatively organized in the following sequence:

$$2, 6, 10, 2, 14, 6, 18, 10.$$

This sequence is in excellent agreement with that resulting from a spherical-like (jellium) super-atom:

$$s, p, d, s, f, p, g, d.$$

Hence, and on top of a structurally stable and highly symmetric cluster, the 68 valence electrons of each cage cluster also organize into a spherical closed-shell electronic system. Consequently these cages qualify as 'double magic'.

3.2. The bulk phase

We investigate now the possible stability of bulk forms of the cluster assembled materials. We restrict our analysis

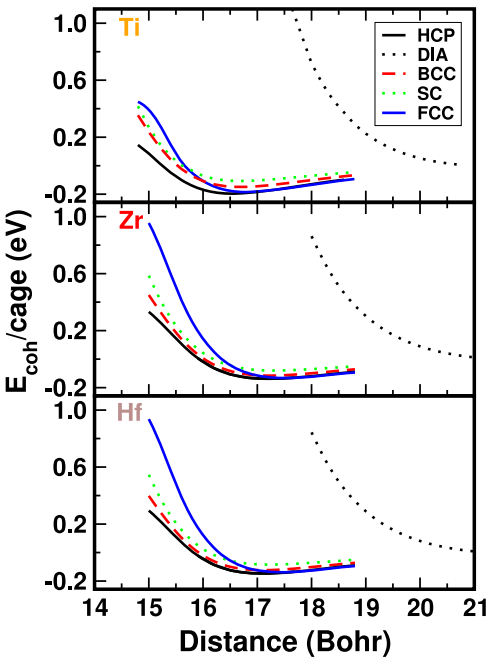

Figure 4. Cohesive energy as a function of inter-cage distance for bulk structures of X@Si_{16} clusters with X = Ti, Zr, Hf. For all crystal structures, nearest neighbour cages are all at the same distance from any focal cage (for the HCP structure $c/a = \sqrt{8/3}$, see main text for details). The curves for the HCP, FCC, BCC and SC are drawn with solid lower (black), solid upper (blue), dashed (red) and dotted (green) lines, respectively. The only curve which exhibits no bound state corresponds to the DIA structure, drawn with a (black) dotted line.

to the Frank–Kasper [32] cage structures even though we are aware that other isomers of M@Si_{16} have been reported in the literature [15, 20, 21]. However, no structure of comparable stability has been identified to date with stoichiometry M@Si_{16}. Hence we believe this choice is justified. The existence of a C_{3v} axis in the Frank–Kasper [32] structure may favour the HCP structure, since C_{3v} is the point symmetry group of the crystallographic $P3m1$ hexagonal group; nonetheless we investigated other possibilities. In figure 4 we plot the cohesive energy per cluster as a function of cage–cage distance for the three cluster assembled materials in their different bulk structures—SC, DIA, BCC, FCC and HCP. In all cases, the cohesive energy curves for the SC, BCC, and FCC structures exhibit well defined minima around 17 bohr. They are, however, less stable than the HCP structure. An entirely different behaviour is found for the DIAmond structure indicating that in all cases this structure is unstable. In figure 5 we show in detail the cohesive energy curves for the three cluster assembled materials in the HCP structure. The curve for HCP Ti@Si_{16} has a minimum for a cage–cage distance of 16.54 bohr and a value at the minimum of only -0.2 eV, indicating that the cages bind weakly. The significant reduction of the binding compared to fullerite [34] (cohesive energy per cluster of -1.6 eV) is related to the role played by the central metal atom, which effectively pulls the valence charge density to within the cage, increasing not only the cluster structural stability but also the HOMO–LUMO gap,

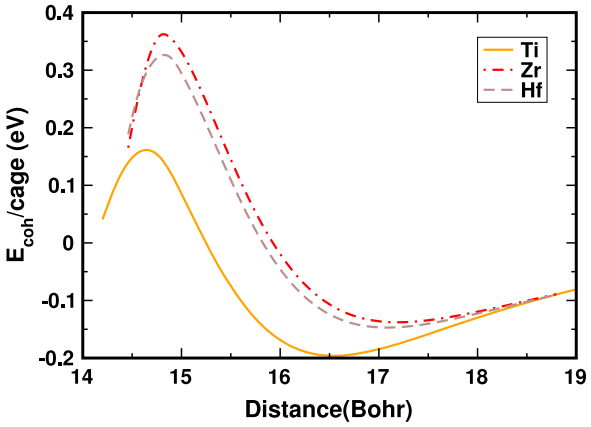

Figure 5. Cohesive energy as a function of inter-cage distance for the HCP molecular solids Ti@Si_{16} (orange, solid line), Zr@Si_{16} (red, dashed-dotted line) and Hf@Si_{16} (brown, dashed line).

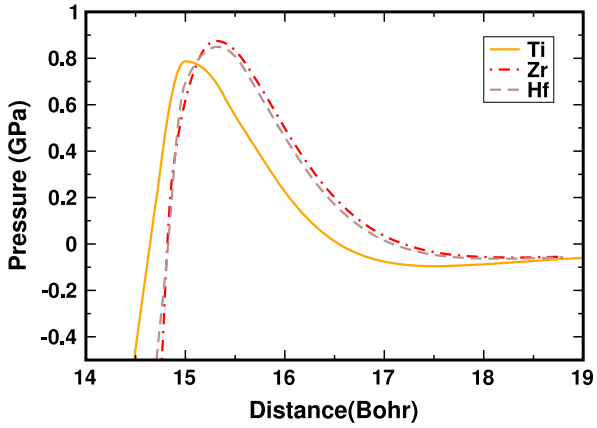

Figure 6. Computed pressure as a function of inter-cage distance for the HCP molecular solids Ti@Si_{16} (orange, solid line), Zr@Si_{16} (red, dash–dotted line) and Hf@Si_{16} (brown, dashed line). The curves were obtained by computing the numerical derivative of the cubic spline fit to the cohesive energy points used to plot figure 5. See equation (2).

Table 4. Lattice parameters for the X@Si_{16} HCP molecular solids with X = Ti, Zr, Hf. Δ is the deviation of the ratio of lattice parameters c/a from the ideal packing value $\sqrt{8/3}$.

X@Si_{16}	a (bohr)	c (bohr)	Δ (%)
Ti	16.54	27.13	0.5
Zr	17.11	27.94	0.01
Hf	16.93	28.14	1.8

Table 5. Bulk modulus for the X@Si_{16} HCP molecular solids with X = Ti, Zr, Hf.

X@Si_{16}	Bulk modulus (GPa)
Ti	1.25
Zr	0.90
Hf	0.97

and therefore reducing its chemical reactivity. The curves for Zr@Si_{16} and Hf@Si_{16} have minima at cage–cage distances of 17.2 bohr and 17.1 bohr respectively. The inter-cage distance in these two structures is ∼4% larger than the one found for HCP Ti@Si_{16}. The values of −0.14 and −0.15 eV at the minimum also indicate that the binding in these bulk materials is weaker than in the bulk Ti@Si_{16}. These results correlate with the fact that both Zr@Si_{16} and Hf@Si_{16} nanoparticles have a cage radius ∼3% larger than Ti@Si_{16}. Indeed, a larger cage radius induces an increase of the inter-cage distance for the cluster assembled materials and also a decrease of the binding between clusters given that the same electronic charge is spread in a larger cluster volume.

Relaxation of both the internal cluster coordinates and the lattice parameters, starting at the minimum structures of figure 5, leads to HCP structures characterized by the lattice parameters summarized in table 4. The atomic rearrangements within each cluster are negligible compared to the isolated cluster geometry, the same applying to the overall changes in cohesive energies. The orientation of the clusters in the Zr@Si_{16} and Hf@Si_{16} HCP structures is compatible with the $p3m1$ crystallographic group and identical to that of Ti@Si_{16} in [25], where it has been explicitly illustrated.

Figure 5 also reveals that, despite the well developed minima in the cohesive energy per cluster, these minima are separated by barriers from other equilibrium structures [25], which turn out to be more stable.

Similar to what was found for Ti@Si_{16} [25], these systems will relax to an amorphous structure where silicon atoms of neighbouring cages bind covalently when subjected, e.g., to very high pressures. This covalent binding leads to an absolute increase of the cohesive energy per cluster to −2.2 eV. However, from figure 5 it is apparent that the values of the barrier maxima for both Zr@Si_{16} and Hf@Si_{16} are larger than the 0.16 eV found for Ti@Si_{16}. This translates into an increase in the applied pressure necessary to drive the Zr, Hf@Si_{16} bulk materials away from their metastable equilibrium HCP structure. Fully unconstrained geometry relaxations, varying both the cluster coordinates and unit cell parameters, starting from a configuration significantly compressed with respect to the equilibrium HCP configuration, show no sign of amorphous transition at normal temperature.

In figure 6 we plot the pressure as a function of inter-cage distance for the three X@Si_{16}, X = Ti, Zr, Hf bulk materials using the data from the cohesive energy curves and equation (2). We found that the maxima of the pressure curves are 0.87 GPa for bulk Zr@Si_{16} and 0.85 GPa for bulk Hf@Si_{16}, values ∼8% larger than the 0.79 GPa obtained for the bulk Ti@Si_{16}, indicating that both bulk Zr@Si_{16} and Hf@Si_{16} are more stable than bulk Ti@Si_{16} against applied pressure. The values for the bulk modulus, B, obtained by fitting the Birch–Murnaghan equation of state, equation (3), to the cohesive energy points are given in table 5.

Quantum Langevin molecular dynamics (QLMD) simulations [30], starting at the Ti@Si_{16} HCP equilibrium structure, suggest that the HCP phase is probably stable at room temperature, as shown in figure 7. QLMD simulations provide a very efficient test of the overall stability of the system, given the feasibility of observing the occurrence of structural phase transitions, whenever they actually take place. QLMD combines

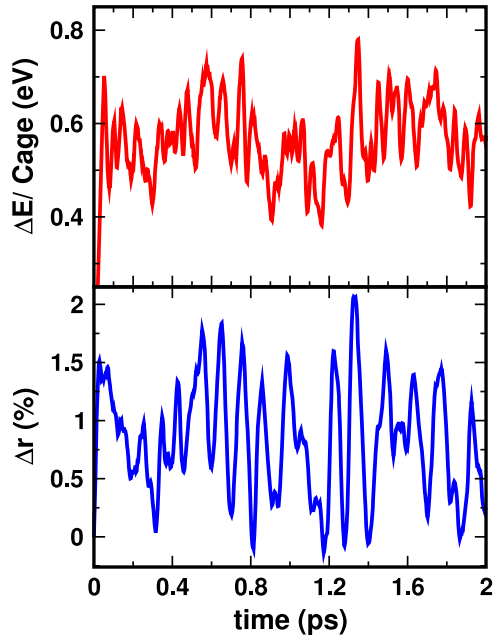

Figure 7. *Upper panel:* change of total energy per cage (with respect to the equilibrium HCP configuration) as a function of time for variable cell-shape quantum Langevin molecular dynamics of bulk-Ti@Si_{16}. The simulation started from the HCP structure at a temperature of 300 K. *Lower panel:* time dependence of the percentage deviation (with respect to the equilibrium value) of the average radius of each cage. The results show the small amplitude of the oscillations taking place at room temperature, and suggest the probable stability of this material. The time step used in each iteration is 2×10^{-15} s, and the simulation ran for a total of 2×10^{-12} s.

some of the advantages of Metropolis Monte Carlo (MC) and MD simulations. By exploiting the energy gradient the atoms move collectively to the minima thereby efficiently sampling the configuration space. This is generally more efficient than a MC procedure where the position of a single atom is updated at each step, followed by a recalculation of the energy. The evaluation of the gradients of the energy, i.e. atomic forces and stress are performed at almost no cost once the energy is determined.

The starting point of the simulation is the equilibrium HCP structure previously determined. Each atom was given an average initial kinetic energy corresponding to a temperature of 300 K. Throughout the simulation the system was in contact with a heat bath at a constant temperature of 300 K. In the top panel we depict the energy difference (per cage, in eV) between the actual configuration at time t and the equilibrium configuration, where one can observe small oscillations around an average energy value reflecting the fact that the crystal is at finite temperature.In the lower panel we depict the time dependence of the deviation from the equilibrium value of the average cage radius (in percentage). Both numbers illustrate the small amplitude nature of the oscillations taking place[1].

[1] The very demanding nature of the computer simulations ultimately dictates the total QLMD simulation time. Besides the large energy cutoff of 30 hartree required to ensure convergence of inter-atomic forces, no symmetry was enforced, such that both atomic coordinates and cell-shape parameters were allowed to vary simultaneously. The total simulation time of 2 ps provides some evidence of the stability of this new molecular crystal. Nonetheless this does not fully warrant, however, its stability.

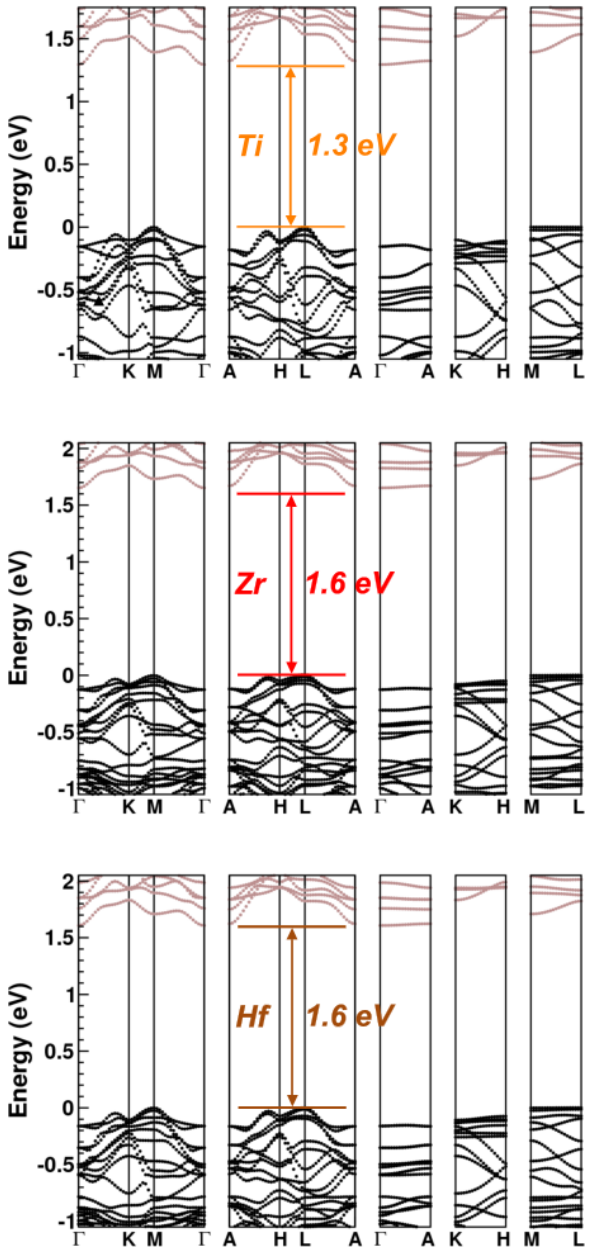

Figure 8. Calculated band structures of bulk X@Si_{16} with X = Ti, Zr, Hf. These molecular materials are predicted to be indirect gap semiconductors. Both Zr@Si_{16} and Hf@Si_{16} have larger band gaps than Ti@Si_{16}.

Finally in figure 8 we show the calculated band structures for the three bulk structures determined above. All three molecular solids are semiconductors with indirect band gaps of 1.3 eV (Ti@Si16) and 1.6 eV (Zr@Si_{16} and Hf@Si_{16}).

4. Conclusions

Making use of first-principles computer simulations in the framework of density functional theory, we have investigated the main structural and electronic properties of the isovalent X@Si_{16} (X = Ti, Zr, Hf) nanoparticles. We showed the feasibility of using these remarkably stable clusters to synthesize molecular solids and we characterized their main

structural and electronic properties. Similar to bulk Ti@Si_{16}, we found that bulk Zr@Si_{16} and Hf@Si_{16} also crystallize in HCP structures with ∼4% larger inter-cage distance, compared to HCP-Ti@Si_{16}. These bulk materials have a phase stability under isotropic compression up to ∼1 GPa and bulk modulus also ∼1 GPa. Fully unconstrained LQMD simulations of the bulk structures suggest their stability at room temperature and normal pressure. Our calculations lead to band gaps of 1.6 eV for Zr@Si_{16} and Hf@Si_{16}. Taking into account that GGA systematically underestimates semiconductor band gaps it is likely that the true band gap is larger than 2 eV.

Synthesis of microcrystallites of these materials should be attainable in laboratory conditions [12, 14].

The results obtained here suggest an interesting hierarchical rationale for the design of cluster assembled materials. Starting from the well known properties of the atoms, one can design target nanoparticles with pre-defined properties which, as such, are the constituent elements of new bulk materials. Furthermore, as shown here, when the nano-cage nucleates around a central atom, one can use at profit the size of the nucleating atom—via isovalent replacement—to manipulate the cage size and, consequently, the bulk lattice, with direct implications on the band gap. This provides an additional degree of freedom which may prove very useful in, e.g., the quest for nano-designed, superconducting alloys. Taking fullerite as a model template, to the extent that doped bulk-X@Si_{16} is superconducting, changing the doping element and the nucleating nano-cage atom may provide additional laboratory knobs to tune the superconducting gap. In this context, it is worth noting that Zr and Hf exhibit properties similar in most respects; however, tables 4 and 5 show that the inter-cage organization in the crystal has subtle differences which may be of relevance. Work along these lines is in progress. We further hope that our results stimulate experiments aimed at synthesizing these materials in the lab [12, 14].

Acknowledgment

Financial support from FCT-Portugal is gratefully acknowledged.

References

[1] Kawazoe Y, Kondow T and Ohno K (ed) 2002 *Clusters and Nanomaterials* (*Springer Series in Cluster Physics*) (Heidelberg: Springer)
[2] Claridge S A, Castelman A W, Khanna S N, Murray C B, Sen A and Weiss P S 2009 *ACS Nano* **3** 244
[3] Schulz M 1999 *Nature* **399** 729–730
[4] Markoff J 2007 *Intel Says Chips Will Run Faster, Using Less Power* (New York: New York Times)
[5] Beck S M 1989 *J. Chem. Phys.* **90** 6306
Beck S M 1987 *J. Chem. Phys.* **87** 4233
[6] Beck S M 1993 *Adv. Met. Semicond. Clusters* **1** 241
[7] Hiura H, Miyazaki T and Kanayama T 2001 *Phys. Rev. Lett.* **86** 1733
[8] Ohara M, Koyasu K, Nakajima A and Kaya K 2003 *Chem. Phys. Lett.* **371** 490
[9] Koyasu K, Akutsu M, Mitsui M and Nakajima A 2005 *J. Am. Chem. Soc.* **127** 4998
[10] Jaeger J B, Jaeger T D and Duncan M A 2006 *J. Phys. Chem.* A **110** 9310
[11] Janssens E, Gruene P, Meijer G, Wöste L, Lievens P and Fielicke A 2007 *Phys. Rev. Lett.* **99** 063401
[12] Koyasu K, Atobe J, Akutsu M, Mitsui M and Nakajima A 2007 *J. Phys. Chem.* A **111** 42–9
[13] Furuse S, Koyasu K, Atobe J and Nakajima A 2008 *J. Chem. Phys.* **129** 064311
[14] Lau J T *et al* 2009 *Phys. Rev.* A **79** 053201
[15] Kumar V and Kawazoe Y 2001 *Phys. Rev. Lett.* **87** 045503
[16] Kumar V and Kawazoe Y 2002 *Phys. Rev. Lett.* **88** 235504
[17] Lu J and Nagase S 2003 *Phys. Rev. Lett.* **90** 115506
[18] Reveles J U and Khanna S N 2006 *Phys. Rev.* B **74** 035435
[19] Guo P, Ren Z Y, Yang A P, Han J G, Bian J and Wang G H 2006 *J. Phys. Chem.* A **110** 7453
[20] Torres M B, Fernández E M and Balbás L C 2007 *Phys. Rev.* B **75** 205425
[21] Bandyopadhyay D 2008 *J. Appl. Phys.* **104** 084308
[22] Gueorguiev G K and Pacheco J M 2003 *J. Chem. Phys.* **119** 10313
[23] Zorriasatein S, Joshi K and Kanhere D G 2007 *Phys. Rev.* B **75** 045117
[24] Pacheco J M, Gueorguiev G K and Martins J L 2002 *Phys. Rev.* B **66** 033401
[25] Reis C L, Martins J L and Pacheco J M 2007 *Phys. Rev.* B **76** 233406
[26] Perdew J P, Burke K and Ernzerhof M 1996 *Phys. Rev. Lett.* **77** 3865
[27] Troullier N and Martins J L 1991 *Phys. Rev.* B **43** 1993
[28] Gonze X *et al* 2002 *Comput. Mater. Sci.* **25** 478–92
[29] Gonze X *et al* 2005 *Z. Kristallogr.* **220** 558–62
[30] Binggeli N, Martins J L and Chelikowsky J R 1992 *Phys. Rev. Lett.* **68** 2956–9
[31] Birch F 1952 *J. Geophys. Res.* **57** 227
[32] Frank F C and Kasper J S 1958 *Acta Crystallogr.* **11** 184
Frank F C and Kasper J S 1959 *Acta Crystallogr.* **12** 483
[33] Kugler S *et al* 1993 *Phys. Rev.* B **48** 7685
[34] Troullier N and Martins J L 1992 *Phys. Rev.* B **46** 1754